ELSEVIER

Polymer 41 (2000) 8887–8895

polymer

www.elsevier.nl/locate/polymer

Structural development during the early stages of polymer melt spinning by in-situ synchrotron X-ray techniques

J.M. Schultz[a], B.S. Hsiao[b], J.M. Samon[a]

[a]*Department of Chemical Engineering, University of Delaware, Newark, DE 19716, USA*
[b]*Chemistry Department, State University of New York at Stony Brook, Stony Brook, NY 11794, USA*

Manuscript prepared in memory of Prof. Andrew Keller

Received 16 September 1999; received in revised form 4 February 2000; accepted 5 February 2000

Abstract

Recent results from melt spinning of several polymers (nylon 6, polyethylene, poly(vinylidene fluoride) using in-situ simultaneous synchrotron small- and wide-angle X-ray scattering (SWAXS) techniques are summarized. Here, mechanisms of early stages of structural and morphological development during crystallization under melt flow are probed. We find that a model consisting of the formation of defective shish-like structures, followed by the formation of kebab crystals is most consistent with our results. We have further verified that the defective shish structure cannot be detected by the wide-angle X-ray scattering (WAXS) technique, but is visible by small-angle X-ray scattering (SAXS). This model has been proposed by Keller et al., for structural development during elongational flow. © 2000 Elsevier Science Ltd. All rights reserved.

Keywords: Fiber spinning; In-situ study; Synchrotron X-ray

1. Introduction

It has been well documented that oriented polymers crystallize more rapidly than unoriented ones, partially because orientation lowers the entropy of the amorphous chains so that the entropy decrease upon crystal nucleation, ΔS_N, decreases. Thus, the free energy increase to form a critical nucleus, ΔG_N, becomes smaller and the rate of nucleation becomes greater [1,2]. However, our current understanding of the role of molecular orientation on polymer crystallization is still incomplete. Many questions about detailed crystallization mechanisms during flow exist. Perhaps the most logical description of orientation-induced crystallization in flexible chain polymers was offered by Keller and coworkers [3–6]. They argued that during flow, only a fraction of the chains with sufficiently high molecular weight can be oriented at any given strain rate. The relationship between the critical strain rate $\dot{\epsilon}_c$ and the molecular weight M during extensional flow can be expressed as:

$$\dot{\epsilon}_c \propto M^{-\beta} \tag{1}$$

where β is a constant with a value about 1.5 for polymer solution, and is unknown for polymer melt. This expression indicates that during flow, there is a critical strain rate for a given molecular weight or a critical molecular weight for a given strain rate. Only chains longer than M will remain oriented, where the rest of the chains will be unoriented due to rapid relaxation. The often-observed shish–kebab morphology in crystalline polymers formed under flow is consistent with this model [3]. The formation of shish can be attributed to the crystallization of extended highly oriented chains, with relatively little back-folding, and the formation of the kebab can be attributed to the crystallization of unoriented or less oriented chains, with substantial chain-folding.

The process of polymer melt spinning is essentially a nonisothermal crystallization process during extensional flow. Advances in the study of structural and morphological development of melt-spun polymer fibers over the past several decades (e.g. Refs. [7–10]) are notable. However, the early stages of crystallization and morphological development are still not known. A thorough review of the orientation development and crystallization behavior during the melt spinning of polymer fibers can be found in Ref. [11]. Recently, Zachmann and coworkers have used synchrotron small-angle X-ray scattering (SAXS) and wide-angle X-ray diffraction (WAXS) (in separate measurements) to follow the structural changes during melt spinning of poly(vinylidene fluoride) (PVDF) [12,13]. They have reported that the SAXS peak appeared before crystalline

E-mail address: schultz@che.udel.edu (J.M. Schultz).

PII: S0032-3861(00)00232-9

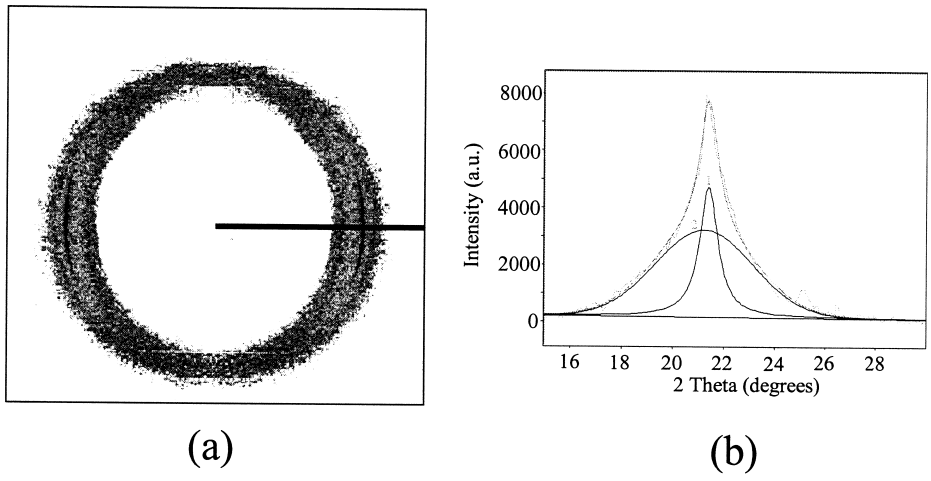

Fig. 1. (a) On-line two-dimensional WAXS pattern for a take-up speed of 50 m/min at a distance of 65 cm from the spinneret. The fiber axis is in the vertical direction. (b) One-dimensional equatorial scan of the 2D WAXS pattern.

WAXS reflections, which indicates that density fluctuations are present prior to crystallization. This phenomenon has also been seen by Ryan et al. in an extrusion study of isotatic polypropylene (iPP) [14]. It has been suggested that this behavior may be due to a spinodal-like decomposition of the amorphous phase into material with a smoothly modulated, periodic density distribution [15–17]. The amplitude of the periodic modulation increases with time and temperature. This observation is a highly contested point in the current literature for it has been pointed out that the result might be a result of experimental data analysis artifacts [18].

In this article, recent melt spinning results of several polymers: nylon 6, polyethylene (PE) and PVDF using simultaneous synchrotron SAXS and WAXS techniques obtained in our laboratories are summarized. Our objective here is to explore the early stages of structural development prior to crystallization during the spinning process.

2. Experimental

The nylon 6 sample was produced by Radici Group Plastics and is commercially known as "Radilon S 38 FL1 Nat.". Its relative viscosity measured in 95.7% H_2SO_4 at 20°C ($c = 1$ g/dl) is 3.90 and its melting temperature is 221.5°C (DSC). The approximate M_w is 25,000, with M_w/M_n between 2.2 and 2.3, and a maximum residual monomer content of 0.25%. Its glass transition temperature after being dried in a vacuum oven at 110°C for 24 h is 45.8°C. The PE is commercially known as "ELTEX A 4009" (Solvay) and is classified as high density PE (HDPE), having an approximate weight average molecular weight of 140,000 g/mol and M_w/M_n in the range of 4–5. Its melting temperature is approximately 130°C. The PVDF sample "SOLEF 6010/0001" (Solvay) has a melt flow index of 17 (at 230°C). Its weight average molecular weight was in the range of 100,000 g/mol and M_w/M_n is approximately 2. Its melting temperature is about 170°C.

The melt-spinning apparatus consisted of a 20 mm diameter single screw extruder attached to a metering pump. The extruder and metering pump were mounted on a horizontal platform that could be translated in the vertical direction. The polymer was extruded through a single hole spinneret die with a diameter of 1.5 mm. Distances along the fiber ranging from 30 to 87 cm from the spinneret could be examined on the spinline using this apparatus. A small ceramic guide and roller wheel was used to minimize fiber movement and vibration.

The SAXS and WAXS measurements were performed at the A2 polymer beamline at the Hamburg Synchrotron Radiation Laboratory (HASYLAB), DESY in Hamburg, Germany. The chosen wavelength was 1.54 Å. The primary beam was rectangular in shape with approximate dimensions of 2×4 mm^2 with its long axis being perpendicular to the fiber direction. The primary beam intensity was monitored by an ionization chamber and the intensity of the beam after passing through the sample was measured by a pin diode that also acted as a beamstop. The sample-to-detector distances for the SAXS and WAXS measurements were 139.5 and 8.0 cm, respectively. The scattering patterns were corrected for fluctuations of the primary beam over time by dividing the scattered intensity by the intensity of the primary beam. All scattering patterns were also normalized for varying collection times. The applied spinning temperature is about 30°C above the nominal melting temperature of the polymer.

The SAXS and WAXS data collection was handled in two different ways. First, two imaging plates were used to capture two-dimensional (2D) images. Collection times were varied to maximize the collected intensity. The second detection method involved the simultaneous use of a 2D 256×256 channel wire detector to collect SAXS images and a one-dimensional (1D) position-sensitive wire detector

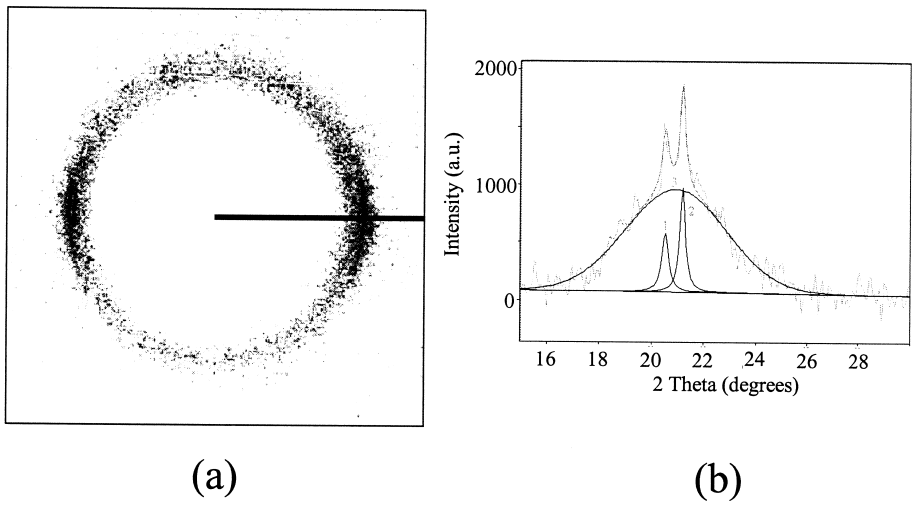

Fig. 2. (a) On-line two-dimensional WAXS pattern for a take-up speed of 50 m/min at a distance of 85 cm from the spinneret. (b) One-dimensional equatorial scan of the 2D WAXS pattern.

(512 channels) to record a 1D slice of WAXS data. This 1D detector was positioned along the equator of the PVDF fiber and along the meridian for PE. The collection time for both the 2D and 1D detectors was 300 s. The patterns from the imaging plates were used mainly for qualitative analysis due to their high spatial resolution and large dynamic range. The wire detector data was used for quantitative analysis in the PE and PVDF experiments. No SAXS measurement was carried out during the nylon 6 study.

3. Results and discussion

3.1. Nylon 6

Figs. 1 and 2 show two types of 2D WAXS patterns collected during spinning at different distances from the spinneret at a take-up speed of 50 m/min. Near the spinneret, the polymer is amorphous and gives rise to the amorphous pattern. At sufficient distance from the spinneret (~50 cm), a type I WAXS pattern (Fig. 1a) develops first. This pattern represents the structure developed during the initial stage of crystallization. An equatorial slice of the type I pattern is shown in Fig. 1b. Deconvolution of this curve into two contributions is also shown. The broader component is an amorphous halo; the narrower, but nonetheless broad, component could be a reflection from a crystalline phase or from a very dense and partially oriented noncrystalline material. For convenience, we will refer to the latter as “crystalline”. The type I pattern is not observed at any take-up speed higher than 50 m/min. As one continues down the spinline, a type II pattern (Fig. 2a) is seen. The corresponding equatorial slice of this pattern is shown in Fig. 2b, along with its deconvolution into amorphous and crystalline contributions. In both type I and II patterns, there is an absence of any off-equatorial reflections, which indicates

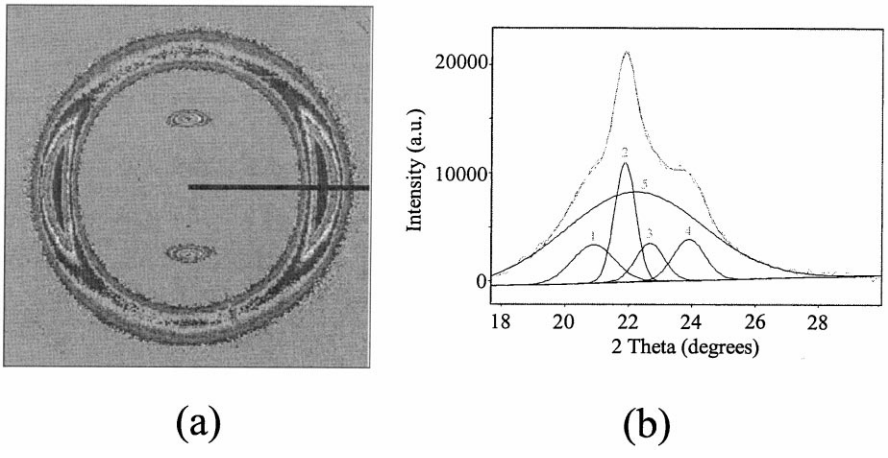

Fig. 3. (a) Two-dimensional WAXS pattern for annealed fiber originally spun with a take-up speed of 400 m/min. (b) One-dimensional equatorial scan of the 2D WAXS pattern.

Table 1
Dependence of the annealed fiber equatorial crystallinity index (α-form, γ-form and total (α + γ)), on the take-up speed during crystallization

Crystal Form	Take-up speed			
	50	100	300	500
α	33	28	18	10
γ	19.5	19	20.5	20.5
α + γ	53	47	38	31

that there are only lateral interactions among the chains along the spinline. In contrast to the type I and II patterns, Fig. 3a shows a representative WAXS pattern for fibers collected after spinning and held at 21°C and 65% relative humidity for 24 hours. This process is later referred to as room temperature annealing. Fig. 3b illustrates the corresponding equatorial slice and the deconvolution of the amorphous and crystalline contributions. From the slice profile, we can identify the alpha (peaks 1 and 4) and gamma (peaks 2 and 3) crystalline forms as well as the amorphous fraction (peak 5). The crystalline peaks of this pattern are attributed to the α200, γ001, γ200, and α002/202 crystal planes, respectively. Table 1 shows the effect of take-up velocity during spinning on the overall (α + γ) crystallinity index, obtained from equatorial diffraction slices, and on the relative contributions of α and γ to that crystallinity. It is seen that the γ content is constant with take-up speed, while the α content increases with decreasing take-up speed. At this relatively low take-up speed, a principal consequence of a lower take-up speed, vis-a-vis a higher, is that a volume element spends more time above its glass transition and thereby can relax the spinline stresses more.

The type I diffraction pattern represents the interactions of oriented polymer chains exhibiting an average correlation distance between them. Two possible models with different chain arrangements have been proposed [19]. The first model consists of nylon 6 chains packed in a hexagonal structure with hydrogen bonding in random directions in the plane perpendicular to the chain direction (fiber direction) and random alignment of carbonyl groups along the chain backbone direction. No three-dimensional (3D) crystallographic registration is developed in this model. The primary reflection is a result of the characteristic hydrogen-bonding interchain distance. The second structural model involves a collection of individual sheets of hydrogen bonded chains. These independent hydrogen bonded sheets do not interact with other sheets in the fiber. A priori, the sheet model should be preferred, as no *hk0* periodicities other than higher orders of the interchain distance can be present, as observed; a hexagonal packing should exhibit other *hk0* periodicities, although the intensities could be low (depending on chain details). Our molecular simulation work using Cerius® Software favors the independent sheet model to explain the type I pattern, using energy minimization to model chain packing; a primary difference of the minimum-energy results is a closer fit of 00l intensities for the sheet model. Although the identification is somewhat problematic, for convenience, we shall refer to the source of the type I reflection as "sheets".

The type II diffraction pattern has been interpreted in a slightly different way. The observed two equatorial peaks indicate that there are two distinct repeat distances between the chains in a plane normal to the chain direction. Similar to type I, the lack of off-equatorial peaks suggests a staggering of carbonyl units between adjacent chains. As the sheets of hydrogen bonded nylon 6 chains begin to interact with their neighbors in adjacent sheets, two repeat distances can be observed: one between the chains in the sheets and one between the sheets. This interaction can be accomplished by the rotation of the carbonyl group by 90° about the chain axis so that there is hydrogen bonding between neighbors in the sheet and between sheets along each chain. After 24 h of conditioning, fully developed 3D crystal structures of the α and γ phases appear, with no remnant of the structures listed above. It is clear that both type I and II structures are metastable and transform into the equilibrium α and γ crystalline forms after conditioning. If the transformation is such that hydrogen bonding occurs only between antiparallel nearest neighbor chains, the α phase is formed. Antiparallel chains are consistent with chain-folding crystals. If the transformation occurs so that hydrogen bonding occurs only between parallel chains, the γ phase is produced. This phase is not consistent with chain-folding, but can be consistent with extended chain crystals (although questions of why only parallel chains should pack together exist).

One possible scenario that can explain the crystallization and structure development during the spinning and conditioning processes is the formation of a shish–kebab structure as proposed by Keller and Kolnaar [3]. During the melt spinning process, the molten polymer chains with a wide distribution of molecular weights, intertwined in a network of entanglements, are under an extensional flow field. As the molecular weight of a chain in the melt increases, the associated density of entanglements and the relaxation time also increase. Chains with lower molecular weights have sufficient time to relax before solidifying, while the longer, higher molecular weight chains do not and remain extended and oriented along the fiber axis upon cooling. Thus upon crystallization, the oriented high molecular weight polymer chains form extended-chain crystals and constitute the shish structures. Upon conditioning, the chain mobility increases and these chains rearrange from the non-equilibrium structure and become the stable γ crystalline form. In this scenario, the remaining material, with lower molecular weights, is present surrounding the highly oriented chains. As chain mobility increases, these chains are able to crystallize by chain-folding into an anti-parallel structure, leading to the α-form crystals and make up the kebabs along the shish. The crystalline polymer that constitutes these kebabs has a preferred orientation in the fiber axis direction as well,

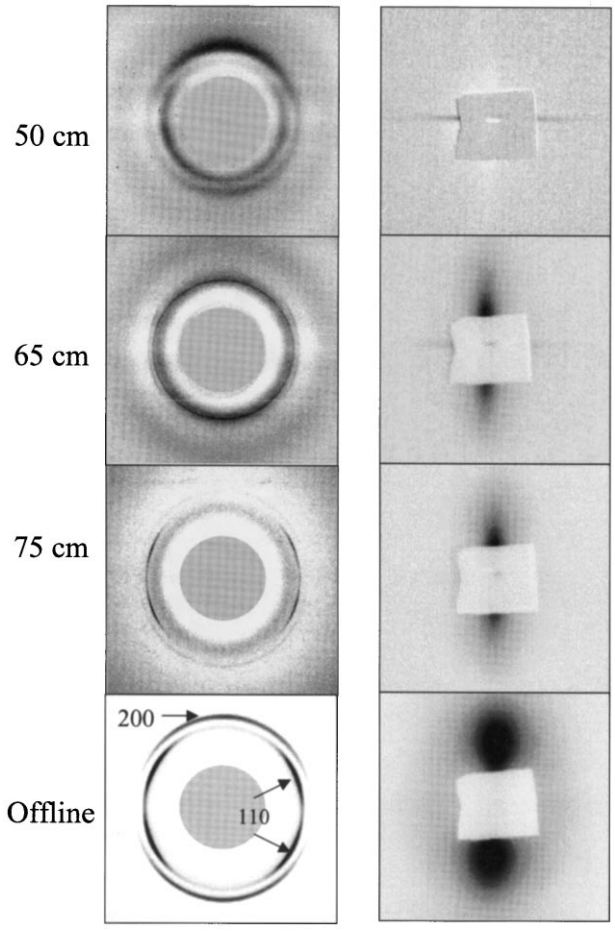

Fig. 4. Two-dimensional SAXS and WAXS images for a variety of spinneret distances at a take-up speed of 61.0 m/min for polyethylene (PE).

probably due to epitaxial growth. Chain mobility is initially affected by the time above T_g during spinning and later by the post-spinning conditioning. The increase in α-form content with decreasing take-up speed is consistent with a model in which the α-form represents the kebab and increases its contribution with increasing time above T_g during spinning.

The shape of SAXS patterns from the annealed fibers, described elsewhere [20], is likewise consistent with a shish–kebab morphology.

3.2. Polyethylene

Fig. 4 shows a series of simultaneous SAXS and WAXS images taken, using image plates, for PE over a range of distances from the spinneret at a take-up speed of 61 m/min. At distances close to the spinneret, the WAXS patterns exhibit an amorphous halo, while no additional scattering is noted in the SAXS patterns. At larger distances from the spinneret (such as 50 cm), an equatorial streak develops first with no indication of crystalline WAXS reflections. As one progresses along the spinline, the SAXS pattern develops a meridianal streak (or lobe) while the equatorial streak begins to diminish in intensity and moves toward the beamstop. By a distance of 65 cm from the spinneret, a nearly isotropic diffraction ring, possibly from a metastable hexagonal phase, is observed. Farther downline, the crystalline 110 reflection (a four-point pattern that is off-equator) is seen. Further along the spinline, the equatorial SAXS streak disappears and the meridianal streak grows in intensity. The 110 reflection intensifies into a well-defined four-point pattern, and the 200 reflection also appears on the meridian. In the off-line samples, examined 24 h after spinning, the SAXS pattern has developed into a two-lobe pattern along the meridian and the WAXS pattern shows a 200 reflection which is still aligned on the meridian and a 110 reflection which is aligned off-equatorially in a four-point pattern. The azimuthal angular position of the maximum intensity of this off-equatorial 110 reflection decreases with increased take-up speed (at a constant distance from the spinneret). The appearance of the four-point 110 reflection and the meridianal 200 reflection have been observed previously [21,22] and were attributed to the radial symmetry of the *b*-axis in the fiber. In this geometry, the *b*-axis is perpendicular to the fiber axis while the *a* and *c* axes are oriented randomly around the *b*-axis. This *b*-axis orientation can stem from a row nucleated shish–kebab morphological model, as described by Keller and Kolnaar [3].

As discussed earlier, crystallization induced by the extensional flow during melt spinning will favorably form extended-chain crystals into a fibrillar structure, the "shishes". Upon a relaxation of the stress, the amorphous material between the shish crystals can epitaxially crystallize as platelet overgrowth perpendicular to the shish direction, the "kebabs". Under weak orientation, the shishes can be very far apart and as the kebabs grow they may twist, as observed under quiescent conditions [3]. The *b*-axes are oriented perpendicularly to the shishes in the direction of twisting kebab growth. Due to the twisting, the *a* and *c* axes achieve random orientation around the *b*-axis.

In the SAXS patterns, different stages of the patterns are observed: equatorial streak, equatorial and meridianal streaks with progressive weakening of equatorial streak, meridianal streak (or lobe) with small trace of equatorial streak, and finally meridianal two-lobe pattern indicative of lamellar structure. These findings are consistent with the proposed model of a shish–kebab structure. As the shishes develop along the spinline, they manifest themselves as an equatorial SAXS streak, the initial shish structure having a higher electron density (close to the crystal density) than the surrounding amorphous phase. These shish are can be sufficiently defective in 3D ordering or sufficiently thin to exhibit no crystalline reflections in the WAXS pattern. As kebabs grow perpendicular to the shish, the combined shish + kebab together have a density higher than the noncrystalline material separating the shish–kebabs and jointly produce an equatorial streak. At the same time a meridianal streak (lobe) becomes evident. As the lateral envelope of the shish–kebab enlarges, the equatorial

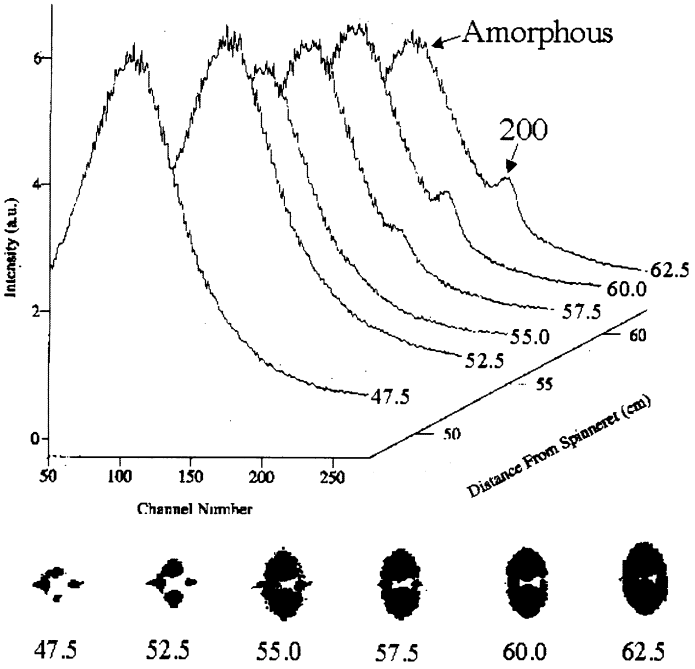

Fig. 5. 1D and 2D wire detector results illustrating SAXS signals appearing before WAXS signals for PE at a take-up speed of 28.6 m/min with the 1D WAXS detector positioned on the meridian. The fiber axis is vertical for the SAXS patterns.

streak must collapse toward the origin, and, before shish–kebabs merge, the intensity must decrease, because of the disappearing volume of contrasting noncrystalline material between the shish–kebabs. Simultaneously, the kebabs, growing more slowly than the shish, are relatively perfect, and WAXS crystalline peaks are seen. Transmission electron microscopy of flexible isotactic polypropylene has shown both shish and kebab structures in the spun fibers [23].

Equivalent results are found using wire detectors for SAXS and WAXS. Fig. 5 shows meridianal WAXS and 2D SAXS images for PE spun at 28.6 m/min. Again a SAXS signal develops prior to observable WAXS, with initially an equatorial streak in SAXS. The equatorial streak fades with position along the spinline as a two-lobe meridianal pattern develops. Fig. 6 shows the small-angle invariant (total integrated area that includes equatorial streak and meridianal streak (lobe) when both are present) as a function of take-up speed and distance from the spinneret for PE. It is interesting to note that the invariant begins at a high value at a short distance from the spinnerets then decreases for all take-up speeds examined, resulting in a minimum value.

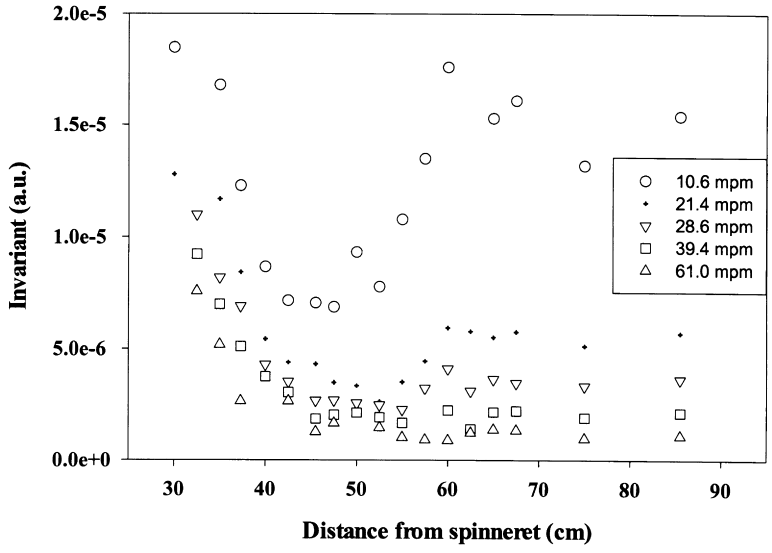

Fig. 6. Small-angle invariant for PE as calculated from the total scattered area under the 2D wire detector.

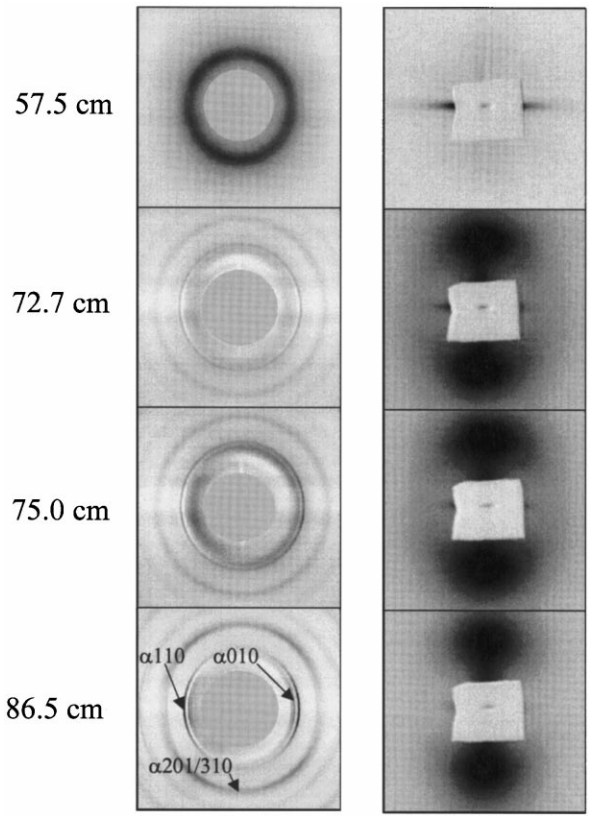

Fig. 7. Two-dimensional SAXS and WAXS images for a variety of spinneret distances at a take-up speed of 10.6 m/min for poly(vinylidene fluoride) (PVDF).

The invariant begins to increase again at the position where the onset of crystallization was observed. The invariant goes through a secondary maximum value and then remains at a steady value. The secondary rise is take-up speed dependent, with the low take-up speeds producing peaking at a level just below their initial maximum and the high take-up speeds barely increasing to a secondary maximum at all. This set of observations is consistent with shish–kebab formation, described as follows. Initially, as shish, and then shish–kebab form and grow radially, an equatorial streak must form and then collapse toward the origin. At the same time that the SAXS equatorial streak is shrinking from the accessible portion of scattering space (thereby decreasing the measured integrated intensity), the stacking and lateral growth of the more perfect kebab crystals promote the gradual appearance of meridianal SAXS lobes and crystalline WAXS peaks. As the take-up speed is increased, the time a noncrystalline volume element spends at temperatures of rapid crystallization decreases and the degree of kebab growth must decrease, resulting in lower degrees of kebab formation and smaller increases in meridianal SAXS intensity with increasing take-up speed.

The results of wire detector experiments in this study confirm that for the case of PE, a SAXS signal appears prior to any identifiable WAXS crystalline reflections [14]. This is illustrated in Fig. 5 that shows both 1D and 2D wire detector results for two typical take-up speeds (28.6 m/min) for PE. These data are similar to those reported above for image plate detection, but cannot be compared directly, because the ambient air was hotter during the wire detector work (since the hutch doors were closed for extended periods and heat from the extruder and instruments built up). For PE at a distance of 55 cm from the spinneret, a small shoulder appears in the meridianal scan (the detector orientation is aligned along the fiber axis) indicating the appearance of the 200 crystalline reflection, while a well-defined two-lobe SAXS pattern is apparent at a distance of 52.5 cm. This observation of a SAXS signal prior to a WAXS signal may be due to either initially small and imperfect shish crystallization or to the poorer detection limit of WAXS (about 1%) compared to that of SAXS (about 0.1%) to determine the crystallinity [18].

3.3. Poly(vinylidene fluoride)

Fig. 7 shows a series of simultaneous image plate SAXS and WAXS images taken for PVDF over a range of spinneret distances at a take-up speed of 10.6 m/min. Qualitatively, at distances very close to the spinneret, the WAXS pattern shows only an amorphous halo, and at this position no SAXS pattern is evident. This is similar to the observation made in PE. Further from the spinneret, an equatorial streak develops in the SAXS pattern, while the WAXS image still only shows an amorphous halo (57.5 cm, for example). Continuing further along the spinline, the WAXS pattern begins to exhibit crystalline reflections. Simultaneously the equatorial streak in the SAXS patterns begins to disappear and a two-lobe meridianal pattern becomes dominant. Still further along the spinline, the crystalline peaks in the WAXS pattern grow stronger while the equatorial streak vanishes entirely from the SAXS pattern. In all but the fastest take-up speed examined (61 m/min), the β-phase of PVDF was not detected, and the crystalline pattern arose entirely from α-phase scattering. At 61 m/min a very weak reflection from the β010 crystal plane was present, but due to its extremely low intensity, it does not contribute significantly to the total crystallinity of the sample.

In Fig. 7, as one moves away from the spinneret there is a distance at which a SAXS signal is detected while the WAXS pattern still exhibits an amorphous halo. These results confirm previous findings that SAXS signals appear prior to WAXS signals [13–17]. However, a further comparison between the kinetics of the equatorial streak and that of the meridianal lobes also suggests that a process of nucleation and growth prevails, rather than the spinodal decomposition. As the equatorial streak always appears prior to the meridianal lobes, we believe that the mechanism of the shish and kebab formation suggested by Keller et al. can best describe the results. During spinning, the shish structures form first and are oriented along the fiber axis as a result of the oriented chains. The shish and subsequent

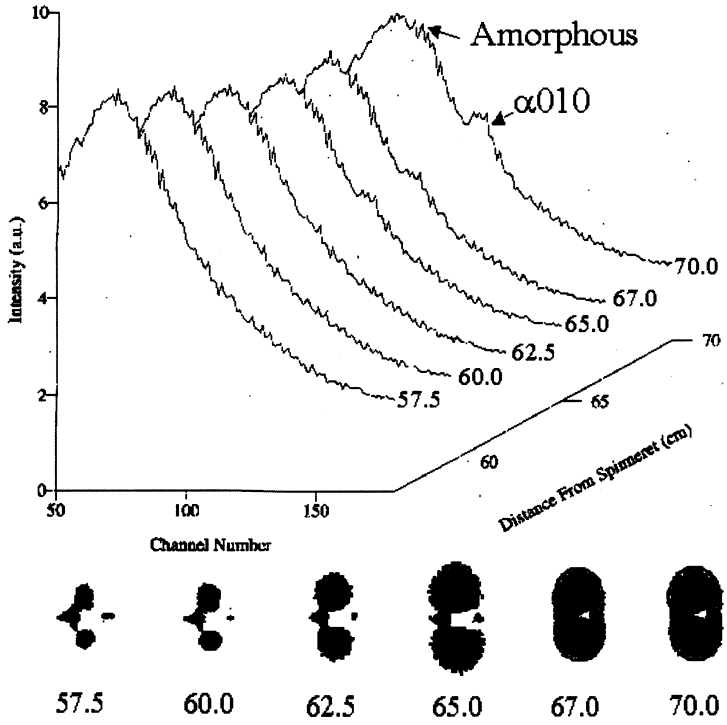

Fig. 8. 1D and 2D wire detector results for PVDF at a take-up speed of 21.4 m/min with the 1D WAXS detector positioned on the equator. The fiber axis is vertical for the SAXS patterns.

shish–kebabs manifest themselves as an equatorial streak. The initial shish is very likely defective in 3D ordering and therefore does not show crystalline reflections in the WAXS pattern. As the periodically stacked and relatively more slowly growing kebabs grow perpendicular to the shish, meridianal SAXS lobes become evident, and WAXS crystalline peaks develop.

Fig. 8 shows both simultaneous 1D and 2D wire detector results for a typical take-up speed (21.4 m/min) during melt spinning of PVDF. A small shoulder appears in the WAXS equatorial scan (the detector orientation is perpendicular to the fiber axis) at a distance of 62.5 cm, indicating the α010 crystalline reflection, while a well-developed SAXS pattern is seen at 57.5 and 60.0 cm. Both of these results reconfirm the SAXS signal (equatorial streak and meridianal lobes) appearing before the WAXS signal. The PVDF invariant has a simpler dependence on spinneret distance. With increasing distance from the spinneret, the invariant increases in a nearly linear fashion (not shown). The invariant at low take-up speeds increases to nearly 2.5 times its original value, while the invariant at high take-up speeds barely increases at all. It appears that the changes of behavior of PVDF represent only the middle section of the invariant evolution in PE.

4. Conclusions

In the present study, the melt spinning of nylon 6, PE and PVDF was studied using simultaneous in-situ SAXS and WAXS techniques. Structure and morphology developments were followed as a function of distance from the spinneret and take-up speed. The following conclusions were reached in examination of the present data:

1. During the spinning of nylon 6, metastable structures develop. The first of these structures appears to represent the formation of individual sheets of hydrogen-bonded chains. Later, interlocking sheets are observed.
2. During storage at room temperature and 65% humidity, the metastable structure transforms into a mixture of α and β crystalline forms. From the details of the SAXS pattern, the nature of the chain packing, and the variation of the relative amounts of α and β after storage, it is concluded that the structure is of the shish–kebab type, wherein the shish is of the β form and the kebab of the α form. It is likely that the initial metastable structure was itself fibrillar.
3. Polyethylene and PVDF exhibit SAXS before WAXS behavior during spinning. This early SAXS signal is in the form of an equatorial streak, not meridianal lobes. This result favors the shish–kebab mechanism proposed by Keller et al. These results do not favor spinodal-like decomposition as a precursor of crystallization.
4. The mechanism for the development of the shish–kebab morphology likely begins with the development of very defective shish-like crystals from

oriented chains of higher molecular weights. The kebabs grow perpendicular to the shish at a later time. The fiber eventually exhibits two-lobe SAXS patterns along the meridian, indicative of a lamellar stacking arrangement.

Acknowledgements

The authors would like to thank the experimental assistance by J. Wu (University of Delaware), F. Yeh (SUNY-Stony Brook), Soenke Seifert (Argonne National Lab.), Norbert Stribeck, Inga Gurke (University of Hamburg) and Cheng Saw (Lawrence Livermore Lab) to this study. The valuable discussions with Profs. David Bassett, Andrew Keller, Bernard Lotz and Richard S. Stein are also acknowledged. The financial supports of this work were by NSF-GOALI grant DMR-9629825 and NSF grant DMR-9732653 (BH).

References

[1] Ziabicki A, Kawai H, editors. High speed melt spinning New York: Wiley, 1985.
[2] Wunderlich B. Macromolecular Physics, 1–3. New York: Academic Press, 1980.
[3] Keller A, Kolnaar HWH. Materials science and technology, a comprehensive treatment, 18. Weinheim: VCH, 1997 (chap. 4, p. 190).
[4] Keller A, Odell JA. Colloid Polym Sci 1985;263:181.
[5] Miles MJ, Keller A. Polymer 1980;21:1295.
[6] Odell JA, Keller A, Muller AJ. Colloid Polym Sci 1992;270:301.
[7] Chappel FP, Culpin MF, Gosen RG, Tranter TC. J Appl Chem 1964;14:12.
[8] Katayama K, Amano T, Nakamura K. Kolloid ZZ Polym 1968;226:125.
[9] Danford MD, Spruiell JE, White JL. J Appl Polym Sci 1978;22:3351.
[10] Wang Y, Cakmak M, White JL. J Appl Polym Sci 1985;30:2615.
[11] White JL, Cakmak M. Adv Polym Technol 1986;6:295.
[12] Hirahata H, Seifert S, Zachmann HG, Yabuki K. Polymer 1996;37:5131.
[13] Cakmak M, Teitge A, Zachmann HG, White JL. J Polym Phys Polym Phys 1993;31:371.
[14] Terrill NJ, Fairclough PA, Towns-Andrews E, Komanschek BU, Young RJ, Ryan AJ. Polymer 1998;39:2381.
[15] Olmsted PD, Poon WCK, McLeish TCB, Terrill NJ, Ryan AJ. Phys Rev Lett 1998;81:373.
[16] Imai M, Kaji K, Kanaya T. Macromolecules 1994;27:7103.
[17] Ezquarra TA, López-Cabarcos E, Hsiao BS, Baltà-Calleja FJ. Phys Rev E 1996;54:989.
[18] Wang Z, Hsiao B, Sirato E, Agarwal P, Srivatson S. Macromolecules, 1999, submitted for publication.
[19] Samon JM, Schultz JM, Wu J, Hsiao BS, Yeh F, Kolb R. J Polym Sci Polym Phys 1999;37:1277.
[20] Samon JM, Schultz JM, Hsiao BS. Polymer 1999;41:2169.
[21] Dees JR, Spruiell JE. J Appl Polym Sci 1974;18:1055.
[22] Nadkarni VM, Schultz JM. J Polym Sci Polym Phys Ed 1977;15:2151.
[23] Schultz JM, Petermann J. Colloid Polym Sci 1984;262:294.